

The Mid-Infrared Instrument for the *James Webb Space Telescope*, II: Design and Build

G. S. WRIGHT,¹ DAVID WRIGHT,² G. B. GOODSON,³ G. H. RIEKE,⁴ GABBY AITINK-KROES,⁵ J. AMIAUX,⁶
ANA ARICHA-YANGUAS,⁷ RUYMÁN AZZOLLINI,^{8,9} KIMBERLY BANKS,¹⁰ D. BARRADO-NAVASCUES,⁹
T. BELENGUER-DAVILA,⁷ J. A. D. L. BLOEMMART,^{11,12,13} PATRICE BOUCHET,⁶ B. R. BRANDL,¹⁴ L. COLINA,⁹ ÖRS DETRE,¹⁵
EVA DIAZ-CATALA,⁷ PAUL ECCLESTON,¹⁶ SCOTT D. FRIEDMAN,¹⁷ MACARENA GARCÍA-MARÍN,¹⁸ MANUEL GÜDEL,^{19,20}
ALISTAIR GLASSE,¹ ADRIAN M. GLAUSER,²⁰ T. P. GREENE,²¹ ULI GROEZINGER,¹⁵ TIM GRUNDY,¹⁶ PETER HASTINGS,¹
TH. HENNING,¹⁵ RALPH HOFFERBERT,¹⁵ FAYE HUNTER,²² N. C. JESSEN,²³ K. JUSTTANONT,²⁴ AVINASH R. KARNIK,²⁵
MORI A. KHORRAMI,³ OLIVER KRAUSE,¹⁵ ALVARO LABIANO,²⁰ P.-O. LAGAGE,⁶ ULRICH LANGER,²⁶ DIETRICH LEMKE,¹⁵
TANYA LIM,¹⁶ JOSE LORENZO-ALVAREZ,²⁷ EMMANUEL MAZY,²⁸ NORMAN McGOWAN,²² M. E. MEIXNER,^{17,29}
NIGEL MORRIS,¹⁶ JANE E. MORRISON,⁴ FRIEDRICH MÜLLER,¹⁵ H.-U. NØ RGAARD-NIELSON,²³ GÖRAN OLOFSSON,²⁴
BRIAN O’SULLIVAN,³⁰ J.-W. PEL,³¹ KONSTANTIN PENANEN,³ M. B. PETACH,³² J. P. PYE,³³ T. P. RAY,⁸ ETIENNE RENOTTE,²⁸
IAN RENOUE,²² M. E. RESSLER,³ PIYAL SAMARA-RATNA,³³ SILVIA SCHEITHAUER,¹⁵ ANALYN SCHNEIDER,³
BRYAN SHAUGHNESSY,¹⁶ TIM STEVENSON,³⁴ KALYANI SUKHATME,³ BRUCE SWINYARD,^{16,35} JON SYKES,³³
JOHN THATCHER,³⁶ TUOMO TIKKANEN,³³ E. F. VAN DISHOECK,¹⁴ C. WAELKENS,¹¹ HELEN WALKER,¹⁶
MARTYN WELLS,¹ AND ALEX ZHENDER³⁷

Received 2014 August 16; accepted 2015 May 07; published 2015 June 5

¹ UK Astronomy Technology Centre, Royal Observatory, Blackford Hill Edinburgh, EH9 3HJ, Scotland, United Kingdom.

² Stinger Ghaffarian Technologies, Inc., Greenbelt, MD 20770.

³ Jet Propulsion Laboratory, California Institute of Technology, 4800 Oak Grove Dr. Pasadena, CA 91109.

⁴ Steward Observatory, 933 N. Cherry Ave., University of Arizona, Tucson, AZ 85721.

⁵ NOVA Opt-IR Group, PO Box 2, 7990 AA Dwingelo, The Netherlands.

⁶ Laboratoire AIM Paris-Saclay, CEA-IRFU/SAp, CNRS, Universit Paris Diderot, F-91191 Gif-sur-Yvette, France.

⁷ INTA, Carretera de Ajalvir, km 4, 28850 Torrejon de Ardoz, Madrid, Spain.

⁸ Dublin Institute for Advanced Studies, School of Cosmic Physics, 31 Fitzwilliam Place, Dublin 2, Ireland.

⁹ Centro de Astrobiología (INTA-CSIC), Dpto Astrofísica, Carretera de Ajalvir, km 4, 28850 Torrejón de Ardoz, Madrid, Spain.

¹⁰ NASA Goddard Space Flight Center, 8800 Greenbelt Rd., Greenbelt, MD 20771.

¹¹ Institute of Astronomy KU Leuven, Celestijnenlaan 200D, 3001 Leuven, Belgium.

¹² Astronomy and Astrophysics Research Group, Department of Physics and Astrophysics, Vrije Universiteit Brussel, 1050 Ixelles, Belgium.

¹³ Flemish Institute for Technological Research (VITO), Boeretang 200, 2400 Mol, Belgium.

¹⁴ Leiden Observatory, Leiden University, PO Box 9513, 2300 RA Leiden, The Netherlands.

¹⁵ Max Planck Institut für Astronomie (MPIA), Königstuhl 17, D-69117 Heidelberg, Germany.

¹⁶ RAL Space, STFC, Rutherford Appleton Laboratory, Harwell, Oxford, Didcot OX11 0QX, United Kingdom.

¹⁷ Space Telescope Science Institute, 3700 San Martin Drive, Baltimore, MD 21218.

¹⁸ I. Physikalisches Institut, Universität zu Köln, Zülpicher Str. 77, 50937 Köln, Germany.

¹⁹ Dept. of Astrophysics, University of Vienna, Türkenschanzstr 17, A-1180 Vienna, Austria.

²⁰ ETH Zurich, Institute for Astronomy, Wolfgang-Pauli-Str. 27, CH-8093 Zurich, Switzerland.

²¹ NASA Ames Research Center, M.S. 245-6, Moffett Field, CA 94035.

²² Airbus Defence and Space, Anchorage Road, Portsmouth, Hampshire PO3 5PU, United Kingdom.

²³ National Space Institute (DTU Space), Technical University of Denmark, Julianne Mariesvej 30, DK-2100, Copenhagen, Denmark.

²⁴ Chalmers University of Technology, Onsala Space Observatory, S-439 92 Onsala, Sweden.

²⁵ 952 Camino Del Arroyo Dr., San Marcos, CA 92078.

²⁶ RUAG Space, Schaffhauserstrasse 580, CH-8052 Zürich, Switzerland.

²⁷ ESTEC, Keplerlaan 1, 2201 AZ Noordwijk, The Netherlands.

²⁸ Centre Spatial De Liège, Avenue du Pre Aily, B-4031 Angleur, Belgum.

²⁹ Department of Physics and Astronomy, The Johns Hopkins University, 366 Bloomberg Center, 3400 N. Charles Street, Baltimore, MD 21218.

³⁰ Airbus Defence and Space, Anchorage Road, Portsmouth, Hampshire PO3 5PU, United Kingdom.

³¹ Kapteyn Institute, University of Groningen, PO Box 800, 9700 Groningen, The Netherlands.

³² Northrop-Grumman Aerospace Systems, One Space Park, Redondo Beach, CA 90278.

³³ Department of Physics and Astronomy, University of Leicester, University Road, Leicester LE1 7RH, United Kingdom.

³⁴ SKA Organisation, Jodrell Bank Observatory, Lower Withington, Macclesfield, Cheshire SK11 9DL, United Kingdom.

³⁵ Department of Physics and Astronomy, University College London, Gower Place, London WC1E 6BT, United Kingdom.

³⁶ Airbus Defence and Space, Gunnels Wood Road, Stevenage, Hertfordshire SG1 2AS, United Kingdom.

³⁷ Paul Scherrer Institut, CH-5232 Villigen PSI, Switzerland.

ABSTRACT. The Mid-Infrared Instrument (MIRI) on the *James Webb Space Telescope* (*JWST*) provides measurements over the wavelength range 5 to 28.5 μm . MIRI has, within a single “package,” four key scientific functions: photometric imaging, coronagraphy, single-source low-spectral resolving power ($R \sim 100$) spectroscopy, and medium-resolving power ($R \sim 1500$ to 3500) integral field spectroscopy. An associated cooler system maintains MIRI at its operating temperature of <6.7 K. This paper describes the driving principles behind the design of MIRI, the primary design parameters, and their realization in terms of the “as-built” instrument. It also describes the test program that led to delivery of the tested and calibrated Flight Model to NASA in 2012, and the confirmation after delivery of the key interface requirements.

Online material: color figures

1. INTRODUCTION

MIRI was the first of the *JWST*’s main science instruments to be delivered to the NASA Goddard Spaceflight Center in the spring of 2012. That delivery marked a major milestone in the work of the consortium of European and US institutes (Rieke et al., 2015a, hereafter paper I) that had designed and built MIRI over a period of more than 10 years. This paper describes the overall instrument design and the development approach. It thereby provides the potential user of MIRI and its data with an insight into the engineering solutions that shape its operation and performance.

The MIRI instrument is the only mid-infrared instrument for *JWST*. To support a full range of investigations, it therefore provides four key scientific functions, whose detailed implementation is described elsewhere: (1) photometric imaging in nine wave-bands between 5 μm and 27 μm over a 2.3 square arcminute field-of-view (Bouchet et al., 2015, hereafter Paper III); (2) low spectral resolving power ($R \sim 100$) spectroscopy of compact sources between 7 and 12 μm (Kendrew et al., 2015, hereafter Paper IV); (3) coronagraphy in four wave-bands between 10 and 27 μm (Boccaletti et al., 2015, hereafter Paper V); and (4) medium spectral resolution ($R \sim 1500$ to 3500) integral field spectroscopy over a 13 square arcsecond field-of-view between 5 and 28.5 μm (Wells et al., 2015, hereafter Paper VI). Each of these capabilities, coupled with the large, cold, aperture of *JWST* will provide a significant advance. To design all of them into a single instrument required novel designs and pushed manufacturing tolerances to the limits. In this paper, we present the common design features of MIRI that support and enable these functions, and discuss how they were integrated into the delivered Flight Model.

A total of three models of the MIRI instrument hardware were built, including the Flight Model (FM) shown in Figure 1 and the subject of this paper and the accompanying ones. The Verification Model (VM) was fully operational (though with reduced imager and spectrometer functionality), and was built to de-risk the opto-mechanical concepts and assembly integration and verification program. The first model, the Structural and Thermal Model (the STM), was built to be thermally and mechanically representative of the FM, to enable early validation of

the thermal design and structural integrity. The STM has subsequently been enhanced with a representative focal plane so that it can be used in the development of the MIRI cooler.

2. INSTRUMENT ARCHITECTURE

MIRI comprises two main components with associated assemblies: the MIRI Optical Bench Assembly (OBA) (§ 2.1) and the MIRI cooler system (§ 5.2), which are operated via separate modules of the MIRI Flight Software running on the *JWST* Science instrument command and data handling system (ICDH).

2.1. Optical Bench Assembly

The OBA consists of the optics module (the OM, shown in Fig. 1), the electrical control and data handling boxes associated

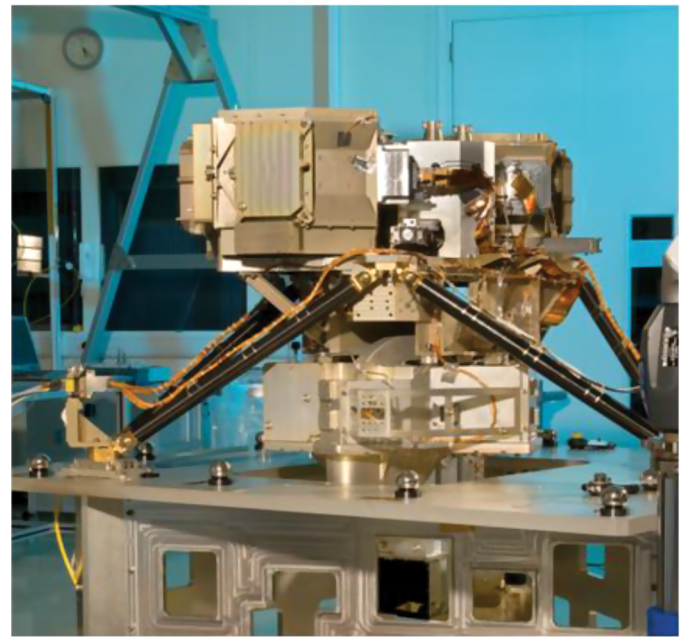


FIG. 1.—The MIRI Flight Model prior to delivery. The optics module structure is aluminum, and it is mounted to *JWST* with a (black) CFRP hexapod truss. See the electronic edition of the *PASP* for a color version of this figure.

with MIRI, which are maintained at 300 K in the separate ISIM Electronics Compartment (IEC; ISIM = Integrated Science Instrument Module), and the necessary interconnecting harnesses.

To combine the science functions into a single package and facilitate an easier assembly, integration and verification program, a modular optical design was chosen where lower level assemblies could be manufactured and their performance verified prior to being brought together in the complete instrument. This approach also enables parallelism and flexibility in the build, test and qualification flow but places stringent requirements on the “systems engineering” component of the project, with interfaces between subsystems needing to be defined, controlled, and

monitored carefully at all stages. The design solution resulted in the OM being split among four main optical modules (subsystems), as shown in Figure 2a and listed as follows:

1. Interface Optics and Calibration (IOC)

2. Mid-infrared imager (MIRIM), interfacing to one Focal Plane Module (FPM) with its detector array. MIRIM encompasses the imager, low-resolution spectroscopy, and coronagraph modes of the instrument.

3. Spectrometer Pre-Optics (SPO)

4. Spectrometer Main Optics (SMO) interfaced to two FPMs with detector arrays; the SPO and SMO constitute the Medium Resolution Spectrometer (MRS).

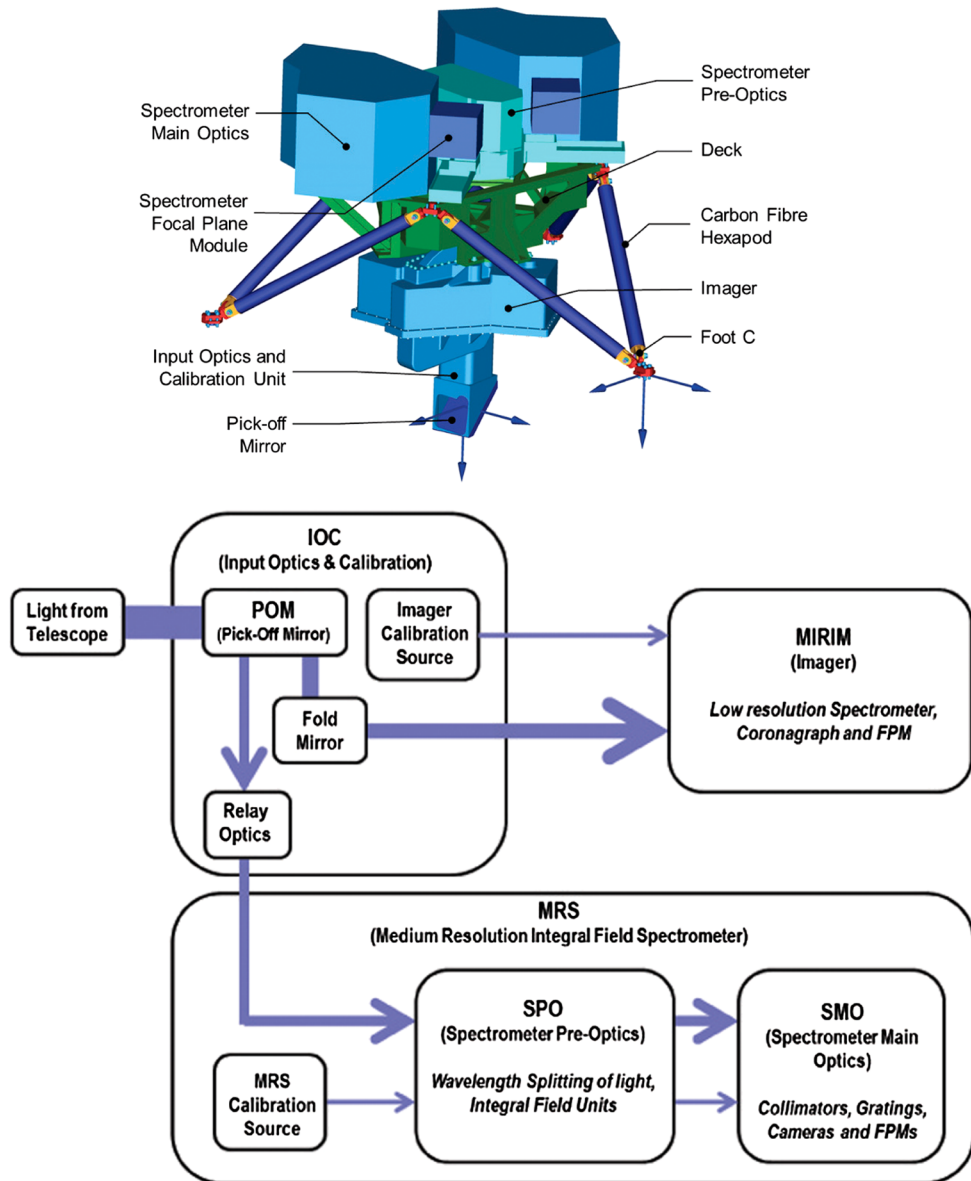


FIG. 2.—(Upper) Overview of the MIRI optical architecture, showing the primary components. (Lower) The science light path (*in blue*) through the MIRI modules. See the electronic edition of the *PASP* for a color version of this figure.

These modules were integrated onto a single structure, the Deck. The completed OM is mounted to the *JWST* ISIM via a carbon fiber reinforced polymer (CFRP) hexapod mounting system (the black rods in Fig. 1). This hexapod thermally isolates the OM from the ISIM, which is passively cooled to about 40 K, while supporting it against the mechanical loads encountered during launch (Jessen et al. 2004).

The MIRI optics take full advantage of state-of-the-art large-format mid-infrared detector arrays. Three focal plane modules (FPMs) with 1024×1024 pixel Si:As IBC detector arrays (Rieke et al. 2015b, hereafter Paper VII; Ressler et al. 2015, hereafter Paper VIII) interface to the OM, with one array dedicated to imaging, coronagraphy, and low-resolution spectroscopy, and the other two used in the medium resolution spectrometer. The FPMs attach to the outside of the optics modules, mating two flat surfaces (with locating fixtures) to provide robust and accurate alignment onto the outputs of the instrument optics.

2.2. Thermal and Cryogenic Considerations

MIRI is the only instrument that must be cooled below the temperature achieved by passive cooling of the ISIM to optimize the detector performance and reduce the thermal background below the detector dark current. The design was developed with thermal constraints as a key driver. The optics module is maintained at a temperature below 7 K by the cooler system. Because of its well understood structural and thermal behavior, aluminum alloy was used to make the supporting structure of the deck and the four optical subsystem modules. The reflective optical surfaces are also of aluminum to simplify the thermo-mechanical design and for the stability of alignment during cool-down. This approach had been proven for other flight and ground based instruments in the mid and far-IR (e.g., IRS and MIPS on *Spitzer*, SPIRE and PACS on *Herschel*, VISIR on *ESO-VLT*, Michelle on *Gemini/UKIRT*) but has been taken to higher levels of precision in MIRI. The instrument optical subsystems and the FPMs are built and aligned at room temperature, and remain aligned when cooled. The designs of both the imaging and spectrometer channels were implemented using the minimum number of low power cryogenic mechanisms (§ 6) to minimize the heat load to the cooler.

3. OPTICAL DESIGN

The optical paths through the instrument are shown schematically in Figure 2b. Both the Imager and Spectrometer channels are fed from a single pick-off mirror in the IOC. The region of the focal plane intended for MIRIM is then selected by a fold mirror close to the telescope focal plane, with light intended for the MRS allowed to pass on through the deck. The positions of the fields in the V2, V3 coordinate system relative to the *JWST* telescope boresight at $V2 = V3 = 0$ are shown in Figure 3.

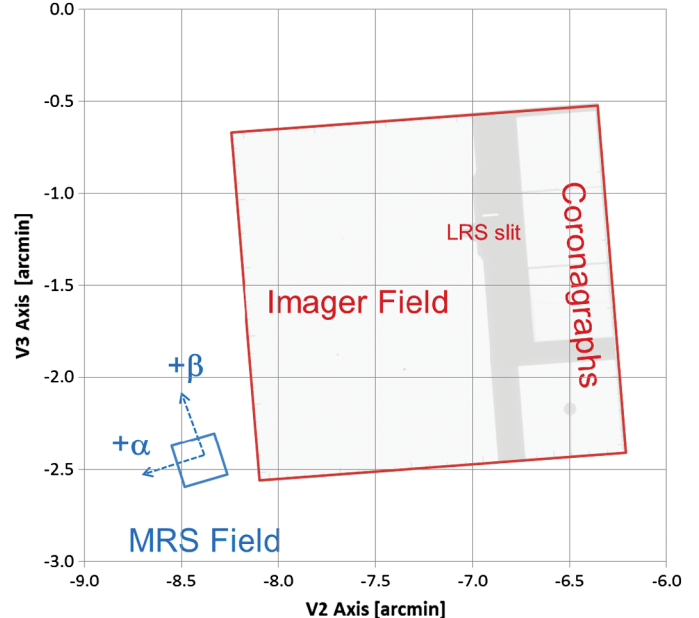


FIG. 3.—The positions of the MIRIM and MRS fields of view in the *JWST* focal plane. The axis is parallel to the along-slice axis of the MRS IFUs. See the electronic edition of the *PASP* for a color version of this figure.

3.1. Imager, Coronagraphs, and Spectrometers

Inside MIRIM, the field-of-view (FOV) is partitioned into three functional areas; imager, coronograph, and low-resolution spectrometer as indicated in Figure 3, enabling all science functions to be supported by a single detector array and a single wheel mechanism. The light is collimated and, at the pupil image formed by the collimator, the single wheel holds the filters for the imager and coronagraphs, a prism assembly for the low-resolution spectrometer, a blank for dark current measurements and a pupil imaging lens. This entrance focal plane is imaged onto the detector using a 3-mirror anastigmat camera with separate areas of the detector being dedicated to the imaging, coronagraphy, and spectroscopy functions. A full description of MIRIM can be found in Paper III.

The MRS (Paper VI) provides diffraction limited integral field spectroscopy over the whole wavelength range from 5 to $28.5 \mu\text{m}$. It consists of two modules shown in Figure 2b—the SPO, which splits the incoming light both spatially, to form an entrance slit for the grating spectrometer, and spectrally into four channels, each of three sub-bands, that are dispersed and imaged onto the detectors in the SMO. The wavelength range is divided into four channels using dichroic mirrors in the SPO; the channels have separate dedicated integral field units and the spectra from each of the four channels occupy half of one of the two MRS detectors. Each channel is split, by a dichroic chain, into three sub-bands that are observed sequentially by rotation of just two mechanisms that carry both the wavelength

sorting dichroics and the dispersion gratings in a very compact and efficient configuration.

3.2. Design Considerations

The limited space allocated to MIRI, plus the need to keep the instrument overall as compact as possible to minimize the radiative heat load on the outer envelope, resulted in the use of relatively fast optical beams. These optics are designed to operate without vignetting and to meet image quality requirements in the presence of up to 4% pupil shear (i.e., the misalignment of the telescope exit pupil and the instrument entrance pupil in units of their diameter) and 2 mm of focus offset, tolerances that became requirements for the optical alignment strategy.

A tolerance analysis showed that MIRI would not need a focus mechanism, so long as tight alignment tolerances were maintained to place the focus position onto the detector and to position MIRI onto the telescope. The design solution to ensure the detector surface was placed correctly was to measure both sides of the flat interface plane and then machine a dedicated “shim surface.” The detector surface position was measured both warm and at cryogenic temperatures to support this approach. To place the output of the optics correctly, an alignment budget was created that gave pupil shear and focus allocations to the subsystems (IOC, MIRIM, SPO, SMO); to each of the interfaces between these subsystems and the deck; and to the ISIM-MIRI hexapod mount. These budgets were set with the intention of achieving an overall focus within 1 mm and pupil shear of no more than 2% for MIRI. The imager and spectrometer were also required to be confocal, which was achieved via the mechanical alignment of the subsystems to the deck. The all aluminum structure means that all subsystem interfaces are direct between mounting pads on each surface, fixing one lateral and two angular degrees-of-freedom, with dowels defining the other two lateral and one angular degrees-of-freedom. The tolerances on these mechanical interfaces and Monte Carlo analysis showed that alignment within budget was possible without recourse to a measure-adjust-measure cycle.

3.3. Alignment into JWST

The optical alignment of MIRI with respect to the telescope requires that the position and orientation of the entrance focal plane and the entrance pupil coincide with the focal surface and exit pupil of the telescope, respectively. Achieving this accurately is key to the scientific performance of the instrument. The positions of the telescope focal surface and exit pupil are well-defined with respect to the telescope optical elements and the mechanical interface between MIRI and the ISIM. However, these definitions are for the in-orbit environment of cryogenic temperature and zero gravity. The design of MIRI needed to take into account the offsets that will occur to the system from the warm as-built conditions found in a terrestrial lab.

On cooling, the distances between the CFRP leg to deck mounting points decrease by the integrated CTE (coefficient of thermal expansion) of aluminum, and the legs shorten by the integrated CTE of CFRP. Analysis showed that the leg/deck interface points would move toward the MIRI/ISIM interface by 0.49 mm on cooling and by only \sim 20 μ m when gravity is reduced to zero. At the same time, cooling of the optical bench causes the pick-off mirror (POM) to move toward the leg/deck interface.

The optical design model of MIRI was used to find by analysis the warm position and orientation of the POM that simultaneously placed the telescope focal plane at the MIRI entrance focal plane and the MIRI entrance pupil and telescope exit pupil at the same location when the system is cooled to its operating temperature. This warm position of the POM was used to inform the design of the IOC and to define the nominal warm positions of the MIRI entrance focal plane and entrance pupil. These were used for alignment verification during the room temperature construction of the optical subsystems and their integration into the OM.

Prior to delivery to NASA the overall alignment of MIRI was checked at room temperature using a NASA supplied reference system called the ASMIF which reproduced both the mechanical and optical interfaces within the ISIM and hence ultimately to the telescope. A series of measurements of pupil shear and focus were made, before and after vibration and cooling to operating temperature, using the references built into MIRIM. The data show that, with measurement uncertainties of 0.35%, the MIRI contribution to pupil shear is 1% and there is no discernable change with changing gravity vector. Focus measurements demonstrated that the MIRI focus is within 0.5 mm of the nominal position. The relative alignment between the entrance pupils of the MRS and MIRIM was measured at cryogenic operating temperature by scanning a point source across one quadrant of the MIRI pupils and correlating the resulting pupil maps to the as-built optical design models of the MRS and MIRIM. No measurable offset between the imager and spectrometer pupils was found. The warm pupil measurements were repeated after delivery using the same fixture to verify that there had been no unexpected issues arising from the transfer. Pupil shear and focus of MIRI relative to the nominal position within ISIM have subsequently been measured at NASA Goddard at cryogenic operating temperature, confirming the warm measurements. All of these results comfortably meet the targets set in the alignment budgets (§ 3.2) to have no significant impact on the performance of MIRI.

The excellent alignment of MIRI determined during test, and the end-end performance discussed in Papers III, IV, V, and VI demonstrate the success of the opto-mechanical approach to the MIRI optical design and alignment.

3.4. Stray-Light Control

Careful attention has been paid to stray-light control. The fine steering mirror (FSM) within the telescope optics is surrounded by a cold stop that provides the defining cold baffle

around the primary mirror. Cold pupil stops are provided within each of the instrument modules. They are slightly oversized to avoid vignetting at the FSM stop even in the presence of a small level of pupil shear, so they provide an additional level of stray-light rejection without affecting the optical path. Papers III and VI describe the stray-light suppression features within the MIRIM and the MRS.

3.5. On-Board Calibration

Stable sources of illumination are needed on-board MIRI for calibration of the instrument's response close in time to an astronomical observation. The requirement is to achieve high signal-to-noise ratio in a short exposure time to derive high spatial frequency flat fields (pixel-pixel gain matrix) and for the source to be sufficiently stable that it can be used to monitor relative detector gain between observations of standard stars. The illumination should therefore be smooth on a spatial scale larger than one pixel and stable for timescales of tens of days.

Identical calibration sources are provided for both the imager and the spectrometer (Glasse et al. 2006). One source is mounted in the spectrometer preoptics and light is injected into the spectrometer optics via a hole in a folding flat mirror. For the imager the source is mounted in the IOC and light injected via a small relay mirror.

Figure 4 shows the source design. Pseudo blackbody radiation is produced by miniature tungsten filament lamps and is rendered uniform by a diffusing surface within an integrating sphere. There are two filaments in each sphere for redundancy. To avoid the steep fall-off at short wavelengths in the blackbody spectrum, the filament must emit with an effective temperature of at least 500 K. In practice, the operating temperature is restricted to less than 1000 K to maximize the filament lifetime.

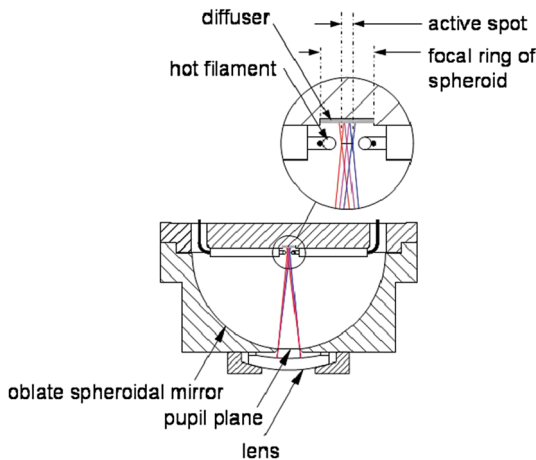


FIG. 4.—Calibration source. A hot tungsten filament illuminates a diffusing surface within an integrating sphere. Light escapes downward through the exit port of the integrating sphere. See the electronic edition of the *PASP* for a color version of this figure.

The long-term stability of the MIRI internal calibration sources was verified during the Flight Model (FM) campaign. The relative flux and repeatability of the source current were measured on eight occasions spread over a period of 46 days. Prior to each measurement the detector was annealed to ensure the results were not affected by its previous history (e.g., latents, image persistency, or other detector issues; Ressler et al. 2015). Signals through the flight filters called F560W, F1130W, F1800W, and F2100W (respectively at 5.6, 11.3, 18, and 21 μm , Bouchet et al. 2015) were measured, to provide a good representation of the wavelength range covered by the MIRI imager.

The relative flux from the source was defined as

$$\phi(\text{filter}, t) = \frac{\varphi(\text{filter}, t)}{\frac{1}{n} \times \sum_{t=0}^n \varphi(\text{filter}, t)} \times 100 \quad (1)$$

where t is the measurement number, and φ is the measured average flux in DN/s within a single photometry region (three boxes of 100×100 pixels² and one of 200×200 pixels² using clean areas of the detector). The standard deviation of the relative flux value over time ranged from 0.411% to 0.270 % depending on the filter. These values were afterward corrected to account for variations in the MIRI Instrument Control Electronics (ICE) calibration source drive current, where the corrections were derived from the accurately sampled current values recorded in telemetry. This correction has been implemented in the Flight Software as an autonomous adjustment, to be applied to the source current once after every switch on.

The final, corrected, calibration source relative flux stability was found to range from 0.039% to 0.203% on a per filter basis, over a 46-day period. This compares very favorably with the accuracy of absolute flux calibration using standard stars which is estimated to be about 1%.

4. MECHANICAL DESIGN

4.1. Mechanical Configuration and Requirements

The MIRI OM is of isothermal construction with the Deck and the optical subsystems all constructed in aluminum alloy and thermally coupled together by bolted interfaces. The combination of this all-aluminum assembly with a simple and efficient CFRP hexapod provided a well understood structure, which could be specified and built to warm dimensions and whose offsets at cryogenic temperatures and under zero-gravity could be accurately predicted.

The main driving requirements for the structure as defined at the outset of the program are listed in Table 1. Sizing of the Deck and the Hexapod elements was driven by these requirements.

The deck is a ribbed and pocketed structure designed to support the various elements with the least expenditure of mass, maximum stiffness, maximum stability and lowest technological

TABLE 1
THE MAIN MECHANICAL REQUIREMENTS FOR THE MIRI STRUCTURE

Parameter	Value
Initial mass budget for the OB	103 kg
Minimum eigenfrequency	50 Hz
Design load (including qualification margin)	18 g
Temperature delta across struts	7 K–35 K
Maximum heat flow across struts	~6 mW for 6 struts
Hexapod mass budget	5 kg
Total primary structure mass budget	18 kg

risk. It is machined in four parts from aluminum alloy 6061. The support for the spectrometer is made as a single part, carrying interfaces for the two Spectrometer Main Optics modules, the Spectrometer Pre Optics, and the Hexapod. It is bolted onto the “lower deck” structure that carries interfaces for the Cooler 6 K Heat Exchanger, the Imager and the Input Optics and Calibration assembly plus some ancillary items. Two struts bolted to this lower deck help to support the wider side extensions to the spectrometer part. The Deck is highly lightweighted and the pocketing is such that there is significant mass only in the regions where the subsystem interface pads locate. The Deck provides the stiffness between the Hexapod apices and was qualified early in the program using the Structural Thermal Model (STM).

4.2. Hexapod Design and Test

The hexapod struts were manufactured from Carbon Fiber Reinforced Plastic (CFRP), which has a favorable combination of strength and low thermal conductivity at cryogenic temperatures. In practice, the hexapod design is stiffness limited, with the driving goal being to minimize the thermal cross section whilst maintaining a margin on the first frequency requirement. The second important design driver for the hexapod struts is buckling. High stiffness and high buckling resistance is achieved by having a high Young’s modulus in the axial direction of the strut. This implies a lower cross section to achieve the first eigenfrequency, a key requirement in Table 1. The chosen design solution for the hexapod is six struts of length 405 mm, diameter 35.5 mm, and 1.2 mm wall thickness. This sizing avoids buckling under the design load and maintains a damage-tolerant wall thickness (Jessen et al. 2004).

The characteristics of the (T300) fiber used in the hexapod are well documented and their use has significant space heritage. This high strength fiber was preferred over a high modulus fiber due to its lower sensitivity to microcracking when cycled to cryogenic temperatures. The resin system is L20/SG. The hexapod strut end fittings and brackets are made from invar for thermo-elastic compatibility with the CFRP.

The Hexapod struts went through an extensive test campaign at strut level to qualify the manufacturing process and confirm strut performance. The performance of the Hexapod and Deck

to provide the required alignment stability and withstand expected launch loads was verified by the Flight Model test campaign.

4.3. Assembly and Alignment

As described in §§ 3.2 and 3.3, the internal alignment of MIRI and the alignment into JWST are achieved by mechanical design and tolerances. To meet the required alignment performance the majority of the structural parts and the mirrors are constructed of two compositionally similar, heat treatable aluminum alloys, 6061 and 6082. Structural and optical components were thermally aged to ensure adequate dimensional stability through subsequent temperature cycling. The optical subsystem modules were mounted on the Deck using bolted and dowel-pinned interfaces. The deck was machined to a surface flatness of 20 μm throughout and the dowel hole location tolerances ranged from 25 μm for the IOC to Deck interface to 90 μm for the SMO to Deck interface. We note that no optical misalignments have been seen during testing of the MIRI Flight Model.

Repeatable mechanical location of MIRI with respect to test and flight interfaces was achieved by means of 6 quarter inch dowel pins, 2 at each hexapod “foot.” For the flight interface to ISIM, these pins locate in a hole and a slot per foot on the ISIM side of the interface.

Conventional practices dictate that ground support equipment to handle the instrument should not occupy flight interfaces. However, transportation (which is the most severe environment seen) was carried out using appropriately protected flight interfaces. This was because of the need to control mass and the presence of an assembled, alignment critical and unconstrained friction locked hexapod. (For all other purposes, there are lifting brackets on the Deck conveniently close to the center of mass.) To avoid accidental damage to the hexapods, a system of “tie rods” was employed to support their feet when the instrument was not mounted at its mechanical interface. The tie rods incorporate length adjustment such that the foot positions could be microadjusted to accommodate manufacturing tolerance differences among the various test, flight, and transport equipment interfaces that the instrument would be mounted to. This system resulted in the overall pupil shear and focus measurements reported in § 3.3.

4.4. Mechanical Loads

The sine loads dictated the design case for the semikinematic MIRI OM, as there are structure resonances in the range 50–100 Hz. Notching of these input loads during test was essential to protect the flexures in the end fittings from damage. The vibration test approach and results are described in detail in Sykes et al. (2012).

The random vibration levels specified at the MIRI instrument interface are relatively low, but nevertheless, attention must be

paid to the critical subassemblies during test to ensure that subassembly specifications are not locally exceeded during instrument test. In particular, the mechanism vibration tests were heavily notched. The notched subassembly test inputs became constraints on the instrument level test as secondary notch limits.

As a basis for interface design and primary notching, limit loads were specified. The MIRI vibration test was a force limited test, meaning that acceleration input was controlled such that the measured force at the interface would not exceed a predetermined maximum. The maximum was set by direct reference to the design load for sine vibration, or by reference to the NASA semi-empirical method (Scharton 1997), in the case of random vibration. By this method, the launch loads were verified to be enveloped without the excessive over testing that would result from applying nominal vibration inputs through the main structural resonances.

5. THERMAL DESIGN

5.1. Overview

MIRI is the coldest instrument on the observatory. The detectors themselves (Papers VII and VIII) must be held at a nominal temperature of 6.7 K with a temperature stability range of 20 mK over a 1000-s exposure. The deck and optics must be held at a temperature below 15.5 K with a stability within a 1 K band to avoid background radiation at long wavelengths that would impact the system sensitivity. It was decided to cool the whole deck and modules attached to it to \sim 7 K, near the detector temperature, to remove temperature gradients and therefore possible sources of misalignment on cooling.

The total heat load from the OM to the cooler heat-exchanger stage during nominal operation must not exceed 46.5 mW. The nominal time-averaged dissipations internal to the OM are determined to be 10.46 mW by correlation of measurements with the MIRI thermal and operating models, leaving about 36 mW maximum for conductive and radiative loads.

To isolate the OM from heat generated in the ISIM that might undermine its thermal design, the OM is enclosed within a cooled shield at a temperature of around 23 K (Fig. 5). The OM is conductively isolated from the ISIM by the hexapod struts visible in Figure 1, which are attached to the ISIM conductive interface, having a temperature of about 40 K. The OM and shield are cooled actively by couplings to the 6 K stage and the 23 K Heat exchanger stage assembly of the MIRI-dedicated cryocooler, which is described below.

5.2. Cooler

The cooling to the detectors, OM, and thermal shield is provided by a \sim 6 K/18 K hybrid mechanical cooler, provided by Northrop–Grumman Aerospace Systems in collaboration with JPL. The system is a further development from the NASA Advanced Cryocooler Technology Development Program (ACTDP),

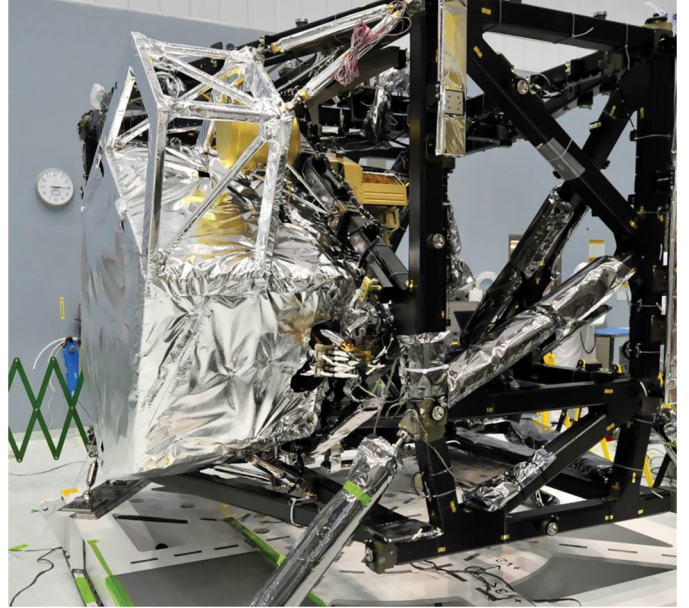


FIG. 5.—MIRI on ISIM and enveloped by the MIRI Thermal Shield, which provides a 23 K radiative environment. See the electronic edition of the *PASP* for a color version of this figure.

which achieved a breakthrough in cooler efficiency while achieving heat lifts of 30 mW from 6 K and 150 mW from 18 K (Ross 2004).

The MIRI Cooler System uses helium as the working fluid and consists of a three stage Pulse-Tube (PT) Precooler that reaches \sim 18 K and a fourth \sim 6 K stage, which is a Joule–Thomson (JT) cooler.³⁸ These two temperatures are made available to the instrument through heat exchangers. It is characteristic of JT devices that their heat lift decreases substantially with increasing precooling temperature. Therefore, a valve bypasses the JT expander to allow the initial cool-down of the instrument by the pulse tube stages. At \sim 18 K, the bypass valve is closed and cooling by the JT expander continues to 6 K. This crossover is termed the “pinch-point” because it is the temperature where there is a minimum in overall heat lift capability.

The cooler system architecture is made particularly challenging since the cooler spans the length of the *JWST* observatory (Fig. 6). The Cooler Compressor Assembly (CCA) is in the *JWST* Spacecraft Bus and is at room temperature, while the Cold Head Assembly (CHA) is mounted on the ISIM structure near the MIRI OM. Both the compressors (PT and JT) are driven

³⁸ A JT cooler works on the familiar principle of allowing compressed gas to expand as it passes through an orifice. Pulse tube coolers (e.g., Radebaugh 2000) produce an oscillating flow through an orifice, or more commonly through a thermal matrix called a regenerator. In the high pressure part of the cycle, warm gas is driven into a reservoir, where it exchanges its heat. In the low-pressure part, the gas flows back through the regenerator and cools it, allowing heat to be removed from the object being cooled.

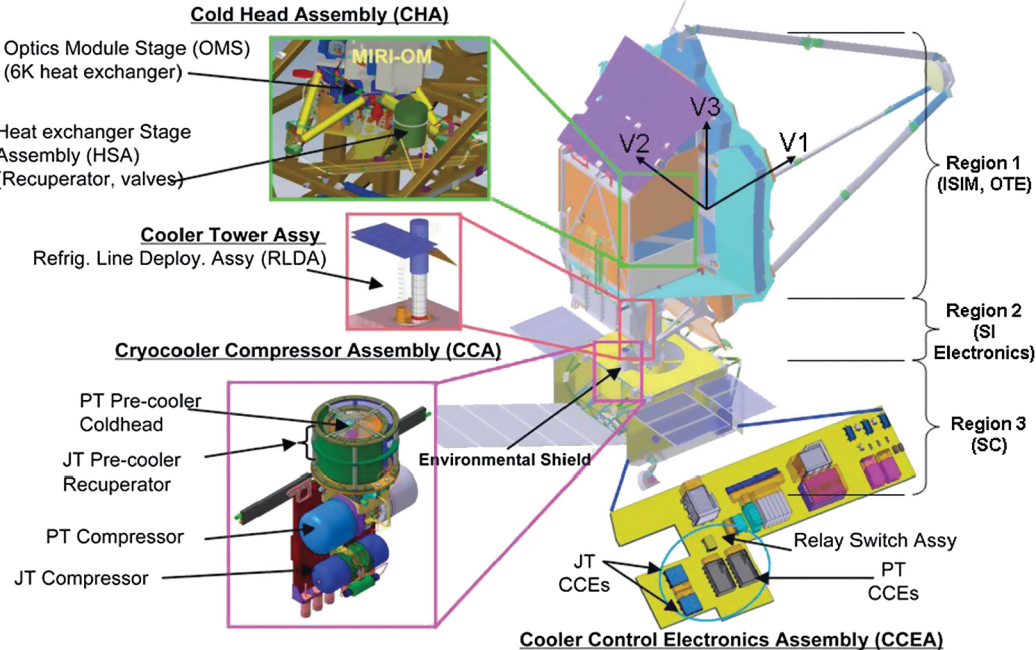


FIG. 6.—MIRI Cooler Components. From Banks et al. (2008). See the electronic edition of the *PASP* for a color version of this figure.

by the block-redundant Cooler Control Electronics Assembly (CCEA) which is located in *JWST* Spacecraft Bus.

The CCA consists of the PT-Pre-cooler, the PT, and JT Compressors (see Fig. 7), plus a radiation shield for the various stages of the pre-cooler. It also supports the stowage structure for the Refrigerant Line Deployable Assembly (RLDA) that runs through the observatory to carry the working fluid from the CCA to the CHA and back. Finally, it includes the structural element that mounts to the spacecraft bus for launch and provides thermal interface to the *JWST* heat rejection system. The refrigerant lines are supported by thermally isolating line supports. The CCEA provides the drive to the compressors and also implements the functions of thermal control, compressor vibration reduction, telemetry generation, and heater and valve control. The CHA contains the Joule–Thomson constriction and has the cryogenic valve that affords switching between the pre-cooler mode and the JT-cooling mode during the MIRI optical system cool-down. Another valve bypasses more of the cold assembly to allow warming the cooler lines for decontamination.

A flight-like CHA was delivered in the 2013 spring. It, along with a ground support equipment pre-cooler, successfully supported the cool-down and operations of the MIRI OS during the ISIM Cryovac1 Test (CV1-RR). The flight CCA and the CCEA are currently in development.

The MIRI cooler system operations will be verified and validated through a series of acceptance test programs followed by a MIRI end-to-end test where a full complement of flight-like cooler hardware will be tested along with thermally representative MIRI hardware (the STM, summarized in § 1). The

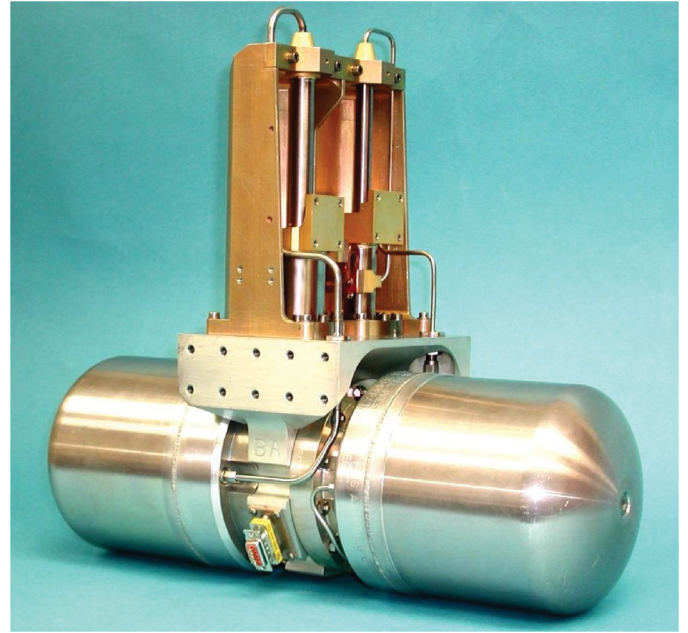


FIG. 7.—Pulse tube cooler (a predecessor of the MIRI flight model). The horizontal cylinders each contain a compressor; the two are driven in opposition to cancel vibration. The cold-stages of the three pulse tubes are connected thermally to the refrigerant line; the third stage is at 18 K. The helium gas is cooled to this temperature as it passes through to the RLDA, from which it is delivered to the optics module and to the Thermal OM shield. See the electronic edition of the *PASP* for a color version of this figure.

end-to-end test will include a flight-like MIRI Thermal Shield, which is also cooled by the MIRI precooler.

5.3. Conductive Isolation

The CFRP hexapod is one of the two main conductive paths between the MIRI OM and the ISIM. The conductance of each strut is about 0.02 mW/K at a mean temperature of 10 K increasing to about 0.06 mW/K at a mean temperature of 40 K (Shaughnessy et al. 2007). Table 2 summarizes the main conductive and radiative heatloads between the MIRI OM and the ISIM or Shield calculated from the correlated thermal model.

Electronic harnesses and a purge pipe also provide paths for conductive heat loads. Harness loads are managed by (1) minimizing of the number of wires required, (2) definition and control of the effective thermal length of the harness between the ISIM heat-sink and the OM deck, and (3) selection of low thermal conductivity materials for construction of the harness (manganin, phosphor bronze, and stainless steel). The purge pipe (which is primarily needed to maintain a clean and dry environment for the wheel lubricants to allow their operation during nonvacuum test activities) is constructed from stainless steel, sized to minimize the conducted load, while allowing the required volumetric flow rate to provide a suitable positive pressure in the instrument.

5.4. Radiative Isolation

With the exception of the optical aperture and access for the cooler heat exchanger, the outer surface of the OM is covered with Single and Multi-Layer Insulation (SLI and MLI) blankets. The SLI is used around the six struts to minimize the conducted heat load from the warmer ISIM. The SLI also encloses harnesses and the purge-pipe that are attached to the struts.

There are two issues regarding MLI for MIRI. First, at low temperatures the thermal isolation achievable is small (e.g., Spradley et al. 1990). Nonetheless, it was decided to encase the OM in MLI both for the thermal gain and as a protective measure for its low-emissivity surfaces. Second, the skin depth of aluminum at a wavelength of 400 μm (by Wien's Displacement Law, corresponding to a temperature of ~ 7 K) is about

0.1 μm . Therefore, the 1000 \AA (0.1 μm) aluminum coating on typical blanket materials can be somewhat transmissive to thermal radiation originating from MIRI and the cold ISIM environment. Consequently, the MLI blankets were constructed using Kapton having a 5000 \AA (0.5 μm) deposition of aluminum on one side. Eight layers are interleaved with crinkled double aluminized Mylar to inhibit conductive heat transfer (net spacers are not used as they are a source of particulate contamination).

5.5. Thermal Control

The detectors are thermally isolated within the FPMs and cooled using a thermal strap of high purity copper from the mount for the detector arrays to a thermal connector on the FPM housings. From this connector, another strap runs approximately 0.5 m from the FPMs to the interface point near the 6 K heat exchanger. This section of strap is constructed from two 2 mm diameter pure (99.99%) aluminum wires that are clamped into specially designed end-fittings to maximize interface conductance. The FPM strap has been sized to allow heating the detectors to keep them warmer than the OM during cool-down (for contamination control), and to permit annealing cycles where the detector temperature is raised briefly to ~ 15 K.

5.6. Contamination Control

As a consequence of the MIRI being colder than the rest of JWST, particular attention was paid in the design to contamination control. There is natural protection from the thermal insulation until the MIRI cooler is activated. Once that occurs, the instrument cools below its surroundings and contaminants from them can collect. Models of the expected JWST outgassing indicate that in the worst case, without protection, a 1.5 μm layer of water ice along with various organic contaminants that are still volatile at 40 K could accumulate on exposed MIRI optical surfaces that are at 7 K. These considerations led to a design with a contamination control cover (CCC) just inside the optical train after the pick-off mirror, which is thermally isolated from the rest of the optics and can be decontaminated by heating. The first cold surface is most vulnerable; the long path of the IOC protects optics further down from transported contaminants when the CCC is open. The CCC design is discussed in § 6.

The Pick-Off Mirror (POM) is the coldest exposed optical surface within the ISIM. It is thermally isolated within the OM structure and fitted with redundant heaters to allow it to be warmed if necessary to drive off contamination (solid N₂, O₂, H₂O, CO₂) that may stick to the mirror. Before the POM heater is activated the CCC is closed to ensure contaminants do not freeze out onto the sensitive internal surfaces.

5.7. Thermal Model Verification and On-Orbit Prediction

A cryogenic test facility was developed at the Science and Technology Research Council's Rutherford Appleton Laboratory

TABLE 2
CONDUCTIVE AND RADIATIVE HEATLOADS

Component	Calculated Heatload (mW)
<i>Conducted</i>	
CFRP Hexapod	7.6
SLI on Hexapod	3.7
Purge Pipe	0.7
Harness	5.8
<i>Radiative</i>	
ISIM to OM	4.7
Shield to OM	0.8

to simulate the environment of the ISIM, including the 40 K radiative environment specified at that time (i.e., excluding the Thermal Shield described above) and the conductive interface with the OM and the 6 K heat-exchanger (Shaughnessy & Eccleston 2009). A 3-month cryogenic test was undertaken on the Flight Model OM to verify and calibrate its performance and to assess the thermal subsystem. Two phases of dedicated thermal tests provided steady-state and transient data for validating thermal models. A close correlation of heat load and temperatures was made to the steady-state data. Heat loads were correlated to within 0.5 mW of measurements and temperatures were correlated to well within 100 mK of measurements.

The nominal steady-state heat load predicted with the correlated model is 33.8 ± 6 mW. This shows a margin of 6.7 mW from the requirement of 46.5 mW, demonstrating that the cooler subsystem will be able to cool and maintain the OM at the required operating temperature.

The in-orbit cool-down prediction using this correlated model is presented in Figure 8. In the model, the ISIM boundary temperatures follow specified profiles, shown in the figure. The temperature of the MIRI shield shown is also interface data for the cool-down prediction and includes the response of the shield to the precooler. The OM is cooled passively until it reaches approximately 100 K, at which point the cooler is activated. A temperature-dependent cooler heat lift was provided for analysis. To demonstrate margin on the requirement, the effective heat lift in the model was reduced by 25%.

The analysis predicts that it takes about 110 days for the OM to reach operational temperatures. The cooler is activated after about 80 days. The inflection in the OM temperature just past 100 days marks the transition through the pinch-point. For contamination control, the OM critical optical elements are required to remain above 165 K until the ISIM is 140 K or below. The analysis confirmed that the OM cool-down lags that of the ISIM and cools below 165 K about 15 days after the ISIM passes 140 K.

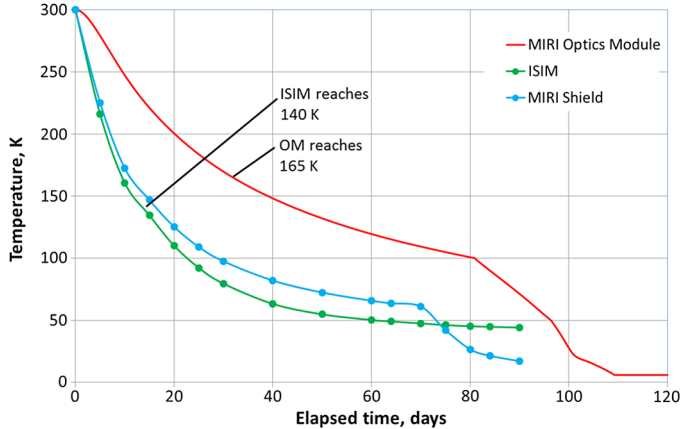


FIG. 8.—Cool-down prediction for MIRI. See the electronic edition of the *PASP* for a color version of this figure.

6. MECHANISM DESIGN

The MIRI Optical System contains four cryomechanisms: (1) an 18 position filter wheel assembly (FWA), mounted in the imager (see Fig. 9); (2) two combined grating/dichroic wheels (DGA-A and DGA-B) with three positions each (see Fig. 10) in the spectrometer; and (3) the contamination control cover (CCC) at the entrance of the optical path of the instrument (see Fig. 11).

The wheel and grating mechanisms lie at the heart of MIRI science operations. The filter wheel assembly is required to achieve a high positional accuracy and repeatability to enable precise alignment of the coronagraph pupil stop. The tight repeatability requirement for the dichroic-grating wheels is derived from the need to move a wheel to select a new wavelength range without recalibrating the wavelength scale.

The wheel and grating mechanisms are all based on the same principle: the wheel bodies are pivoted in a central combined bearing and retained in their optical position by a ratchet system. A brushless (and gearless) central torque motor is used to operate the wheel in an open loop drive. This requires only relatively simple but robust drive electronics. In addition it minimizes the number of harnesses from the warm electronics to the cryogenic part of the instrument and thus the conducted heat load. The chosen wheel design guarantees high precision and highly reliable positioning of the optical elements while using low driving power—in particular zero power during science operation—and therefore low heat injection into the cooled MIRI instrument (more details can be found in Krause et al. [2010]).

Operating the wheels from one position to the next adjacent position takes ~ 8 s in total. This includes ~ 500 ms for motor acceleration and deceleration, ~ 3 s of settling by the ratchet system and ~ 4 s to complete a final position sensor readout to crosscheck that the correct position has been reached. The

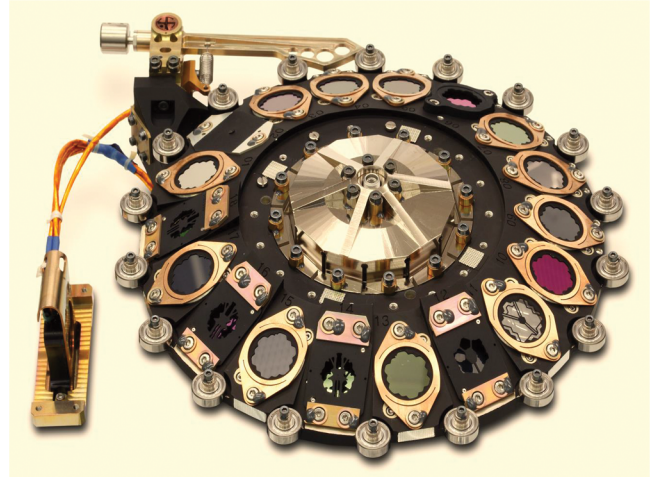


FIG. 9.—The MIRI Filter Wheel Assembly (FWA). See the electronic edition of the *PASP* for a color version of this figure.

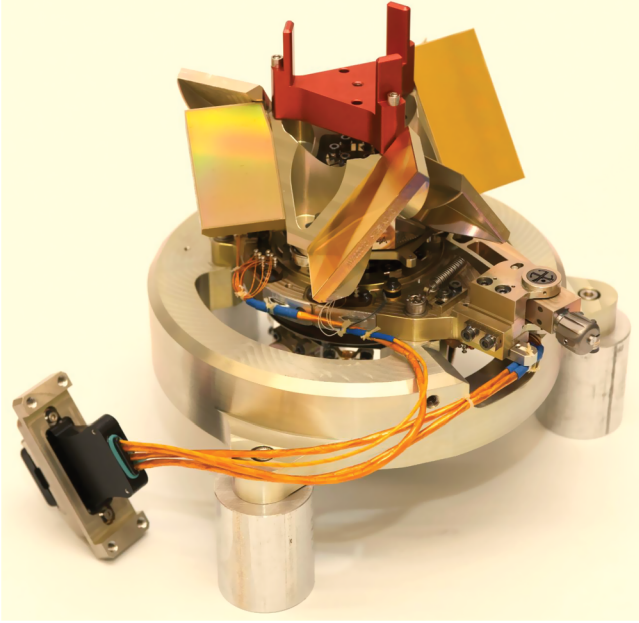


FIG. 10.—Dichroic/Grating Assembly A (DGA-A). See the electronic edition of the *PASP* for a color version of this figure.

final positioning accuracies are $\sim 1''$ for the FWA and $\sim 3''$ for the DGAs.

Since no wheel angle feedback is available during the movement, the precise characterization of the mechanisms and their motors was fundamental to minimize heat load and maximize the reliability of the mechanism movements over their lifetime

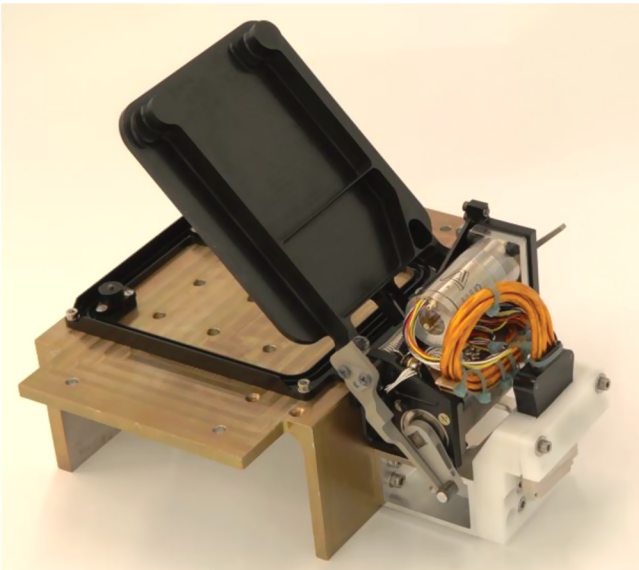


FIG. 11.—Contamination Control Cover (CCC) mounted on a mechanical support. See the electronic edition of the *PASP* for a color version of this figure.

(Detre et al. 2012). This has been achieved and proven over several test campaigns.

The Contamination Control Cover (CCC, Glauser et al. 2008) is a door mechanism located in the Input Optics between the MIRI pick-off mirror and the first fold mirrors (see Fig. 11). The CCC was introduced to protect the instrument against molecular contaminants outgassing from nearby structures after launch, during ISIM cool-down, or during any ground based test campaign. With its contact-free labyrinth seal, the CCC also closes the instrument in an optical sense, blocking any stray-light. Since the CCC operates at the same temperature as the rest of the instrument, it is also suitable to provide a dark environment for internal calibration measurements.

The CCC uses two identical redundant stepper motors that lever the cover toward its open position, while two redundant springs push it toward the closed position. The qualification of this mechanism has shown that the design is highly robust and reliable (Glauser et al. 2008). The molecular throughput has also been measured (Glauser et al. 2009) and shows perfect agreement with theoretical predictions.

7. ELECTRONIC SYSTEMS

The MIRI electronic systems split functionally into the electronics for the MIRI Cooler System that is described in § 5.2 and the MIRI Optical System electronics.

The MIRI Cooler Control Electronics Assembly (CCEA) is a set of independent and dedicated electronics assemblies, which control and drive the Cooler Thermal Mechanical Unit's (TMU) two compressor assemblies—Pulse Tube (PT) and Joule Thomson (JT). These are based on heritage designs currently in other space flight applications and are capable of highly accurate temperature control over the temperature range from 4 to 15 K. The Cooler Control Electronics (CCE) are single-string, but redundant at the box level to enhance reliability and meet the lifetime requirement, and there is a set of primary and redundant JT and PT CCEs for each compressor. A third electronics assembly, the Relay Switch Assembly (RSA), provides the switch to allow the use of either set of cooler electronics to drive the single TMU assembly. The RSA contains latching relays and accepts a pulse command from the spacecraft to effect switching from primary to redundant CCEs, or vice versa. One key function of each JT and PT CCE assembly is to convert, condition, switch, and distribute incoming SC primary bus power, and furnish it in the correct form to drive the various elements of the compressor assembly. Each CCE provides closed-loop control of various compressor and cold head functions, monitors the status of key performance and safety parameters, and communicates with the ISIM Command & Data Handling system host via a MIL-STD-1553B bus. Generally, these control functions involve both analog and digital circuitry and supporting internal software, which also provides automated fault protection.

The MIRI Optical System electronic architecture is summarized in Figure 12. The operation of the instrument is controlled

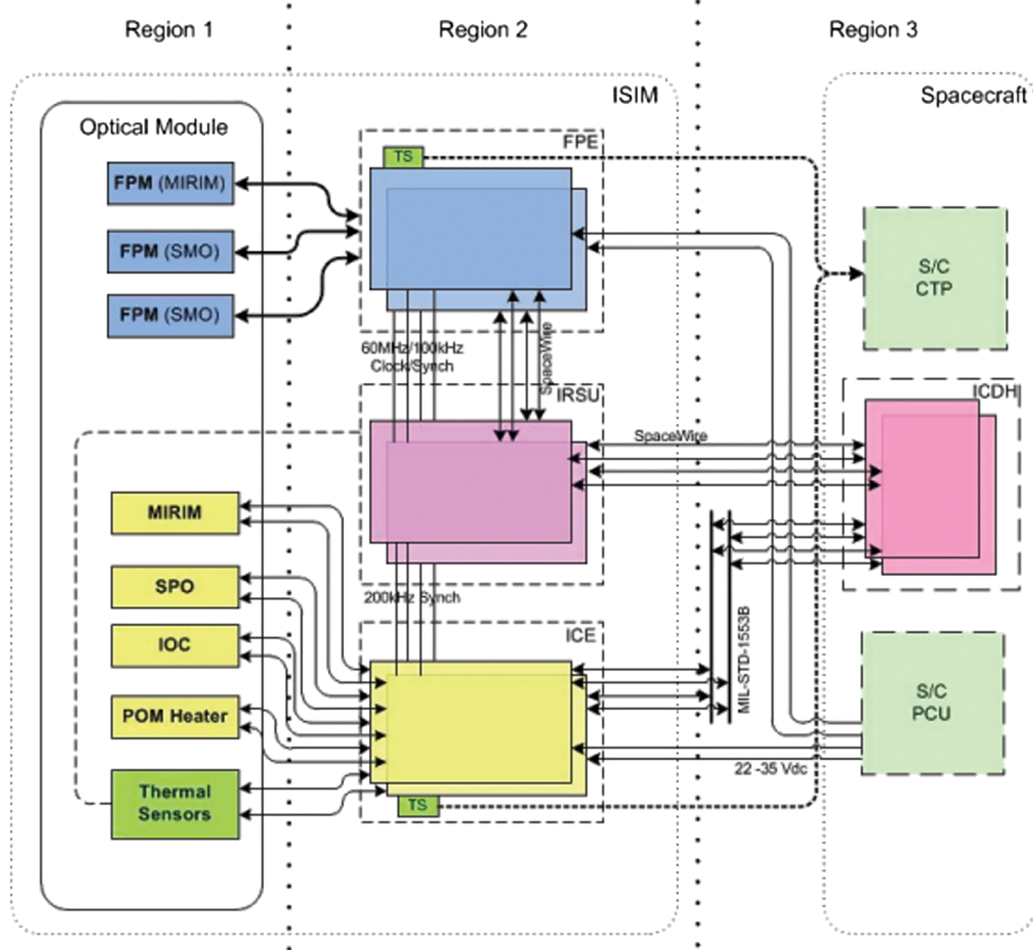


FIG. 12.—Electrical Architecture for the Optical System. See the electronic edition of the *PASP* for a color version of this figure.

by the ISIM Control & Data Handling (ICDH) system via the two discrete electronic boxes; the Focal Plane Electronics (FPE) and the Instrument Control Electronics (ICE). The Spacecraft Power Conditioning Unit (PCU) supplies power directly to each of these units at a nominal voltage of 31V(DC). The FPE and ICE both operate at ambient temperatures (300 K) and are mounted in a dedicated warm region of the ISIM referred to as the ISIM Electronics Compartment (IEC). In addition to the links to the ICDH there are eight spacecraft temperature monitoring sensors for when the instrument is switched off.

The Focal Plane System (FPS), comprising the detector, FPE, and associated harness is described in detail in Paper VIII and so is not discussed further here.

The ICE controls the four mechanisms and two calibration sources discussed above, along with 15 temperature sensors and the decontamination heater. While the mechanisms, sources, and sensors are mounted on the optical bench at ~ 7 K, the ICE is maintained, along with other science instrument electronic boxes, in a separate section of the observatory at an operating temperature of ~ 300 K. The wiring harness connecting

the OM with the ICE uses phosphor bronze for wires with relatively high current (~ 100 mA), whereas stainless steel is used for the low current sensor lines. The ICE has no internal processing capabilities and operates only via command from the JWST integrated science instrument module (ISIM) control and data handling module (ICDH).

The ICE is a fully redundant design with a modular architecture. It has two service modules; “DC/DC” and “TM/TC & Scheduler,” and two application modules; “Motor control” and “Conditioning.” The modules are powered, interconnected, and communicate via a back plane, which also allows for cross strapping of temperature sensors and nonredundant mechanism position sensors, to enable monitoring with either of the two redundant sides of the ICE.

The DC/DC module is responsible for the power supplies handling, accommodating the spacecraft primary power bus (an unregulated 22–35 V power bus).

The TM/TC & Scheduler module interfaces with the ICDH via a 1553 bus and with the application modules via a proprietary media bus implemented on the back plane. As such, it

receives telecommands, then translates and distributes these commands to the relevant application module. It also collects and formats telemetry data, which is then made available for the ICDH. Another function of this module is to drive the back plane relays to select the appropriate routing for the temperature and position sensors.

The Motor control module controls and monitors the drive currents and voltages for one (at a time) of the four MIRI mechanisms. The particular motor and voltage supply (40 V nominal <10 K operation, 80 V room temperature operation) are selected in advance via relays; then the power amplifier controls the coil pair for the selected motor, activating the mechanism. To overcome an environmental failure case of the CCC sticking in the closed position, a special relay setting is available to allow the activation of the two CCC stepper motors at the same time, thereby doubling the opening torque.

The remaining control and monitoring functions of the ICE are provided by the Conditioning module. This module provides the current drive and control for the calibration sources and the decontamination heater. It monitors and provides telemetry data on the temperature and mechanism position sensors. Control of the DC/DC module, synchronization, motor voltage selection and activation is also provided in this module.

8. CONTROLLING MIRI

The MIRI instrument relies on the ISIM to provide all command and control functions for the hardware. These services are provided by the ICDH, which consists of a single-board computer, some basic image processing modules, and several communications interfaces.

The communications links between the ICDH and the MIRI electronics boxes are shared with the other instruments. High-speed data links are provided to the MIRI focal plane electronics over a Spacewire bus, routed via the ISIM Remote Services Unit (RSU). The ICE and CCE (Cryocooler Control Electronics) require relatively low data rates and are linked via the ISIM 1553B bus. The ICDH has further links to the *JWST* observatory and spacecraft systems to allow it to receive commands, and to send science and engineering telemetry to the solid state recorder. Additionally, the ISIM (and hence MIRI) receives all of its electrical power from the spacecraft.

The ISIM flight software (FSW) consists of multiple software modules, each of which has a distinct function. Generic services such as communications, timing, and memory management are provided within the “core” software, as these are required by all of the instruments. Each instrument has one or more dedicated modules for controlling its own functions, which were developed by the instrument teams. These modules use the services provided by the core ISIM software to communicate with the instrument hardware, and to send and receive information from the timeline or ground operator (via the spacecraft and observatory systems).

The MIRI software is split into two separate modules with distinct functions:

1. MIRI Optical System FSW

- a) Command and control the MIRI OBA hardware.
- b) Operate the mechanisms, calibration sources and POM heater via the ICE.
- c) Operate the detectors and their thermal control heaters via the focal plane electronics.
- d) Monitor sensor data (e.g., temperatures) from the OBA.
- e) Maintain OBA hardware safety during commanding of each item.

2. MIRI Cooler FSW

- a) Command and control the cooler system.
- b) Operate all cooler components via the CCE.
- c) Monitor sensor data (e.g., temperatures) from the cooler system.
- d) Maintain cooler hardware safety during operations.

MIRI can receive commands from the ground (via the spacecraft), or from on-board sources such as the science timeline or stored commanding (used for safety-critical actions). Early in-flight operations (such as instrument commissioning) and some regular engineering activities will be carried out by ground operators, normally by using ground scripts to send commands and to verify the telemetry.

Most in-flight MIRI operations will be conducted from the ISIM science timeline, and will be planned well in advance. The timeline will consist of a series of observations, each involving one or more instruments. The specification for each observation is translated on-board into a sequence of instrument and observatory operations (e.g., spacecraft pointings), while the MIRI commands are generated by dedicated on-board scripts for each observing mode. The science timeline execution system is capable of performing a sophisticated level of error checking, to ensure that constraints are enforced and that any errors reported by the instruments are handled appropriately.

Commands are processed in the same way irrespective of their origin, so that only a single interface is needed. Most MIRI commands are reasonably high level, and many of them correspond to individual instrument functions. For example:

1. Set cooler cold-head temperature (set up the cooler in preparation for MIRI operations)
2. Move filter wheel (select the Imager filter required for an observation)
3. Switch on calibration source (in preparation for calibration measurements)
4. Start exposure (begin taking science data with the current detector settings)

The flight software modules are responsible for translating each command into appropriate instructions for the electronics

boxes, and for ensuring that the commands are completed successfully. In addition to the high-level commands, there are lower-level commands to facilitate engineering operations and instrument troubleshooting. There are also many programmable options in the software that can be adjusted (e.g., operating temperature limits, time-outs, etc.), so that any unexpected events during the mission can be dealt with as easily as possible. The flight software modules themselves can also be patched if necessary.

The MIRI and ISIM designs lead to various constraints and limitations on operations. Some of the more significant examples are listed below:

1. The three MIRI detectors can be operated individually or in parallel, but detector settings (e.g., bias voltages) cannot be altered while science exposures are in progress.
2. The MIRI mechanisms can only be operated individually (i.e., in a serial manner).
3. Read-out of virtually all engineering telemetry from the electronics occurs at a fixed cadence of 1 reading every 4 s. Sampling on a finer timescale is only possible for certain mechanism parameters or in engineering modes.
4. Science data read-out is not synchronized to engineering telemetry, and the start time of a science exposure cannot be controlled to better than the detector frame read-out time (typically about 3 s, but can range from ~ 0.1 s to ~ 27 s depending on the observing mode).

9. THE OVERALL TEST AND VERIFICATION OF THE MIRI OPTICAL SYSTEM

The modular instrument design reduced risk for the flight model Assembly Integration and Verification (AIV) because it allowed a series of incremental qualification and performance verification tests to be performed at subsystem level. The three model approach (STM, VM, FM—structural/thermal, verification, and flight models, respectively) proved to work well, with sufficient flexibility to accommodate problem solving throughout the program. The main aims for the STM were to provide an early mechanical qualification of the Primary Structure, thermal model validation and to prove out the test facility prior to the VM test. The VM objective was to verify instrument optical performance at operating temperature sufficiently early to avoid major cost and schedule problems in the event of detected problems requiring extensive FM modifications. The VM testing was split into two campaigns, one to test the instrument optics with a very simple single point simulated *JWST* source and a second more extensive test using the MIRI Telescope Simulator, which also provided feedback to the design of the MTS and to the test plans and scripts for the Flight Model test campaign.

Following integration, the MIRI Flight Model was tested for 1600 hr during 2011 in the test chamber described in § 5.7 and in Shaughnessy & Eccleston (2009). This provided a background radiation environment that was a close analog to the expected on-orbit environment, namely, a near blackbody

emission spectrum with an effective temperature of 40 K. This test campaign was therefore the best opportunity to measure the performance of MIRI prior to launch, especially in the areas of photometric calibration and straylight. Further, this test campaign was the only opportunity to study fully the spectral performance of the MRS before launch.

9.1. The MIRI Telescope Simulator

The MIRI Telescope Simulator (MTS) was the cryogenic optical system developed to generate the illumination sources for MIRI performance measurements. The MTS detailed design is described in Belenguer et al. (2008). In this section, we summarize its major functions and describe the computational model (MTSSim) that was produced to predict its photometric output. At the heart of the MTS was a laboratory standard blackbody whose temperature could be selected in the range 100–800 K. The collimated beam from this source passed through an adjustable iris diaphragm (to set the flux level) before reaching the MTS filter wheel. The wheel included a closed position to block the MTS hot source for background estimation; a clear position for broad band illumination; one long-wave pass filter and one short-wave pass filter for measurement of spectral leaks; and four solid state Fabry–Perot etalons which provided a comb of spectral lines for the wavelength characterization and calibration of the MRS. The output beam from the filter wheel was then presented to an integrating sphere whose spatially uniform output was matched to the input of a Cassegrain telescope (the Main Optical System [MOS]). By inserting a pinhole (one of two mounted on a three axis moveable stage) at this input, the MOS was designed to reproduce the point spread function delivered by the *JWST*. The point sources could be moved to any point within the MIRI field-of-view with an absolute accuracy equivalent to 1 imager pixel, and a relative accuracy of better than 0.1 pixel for small displacements. With the pinhole mechanism driven out of the beam, flood illumination across the full MIRI entrance focal plane was obtained. An infrared LED source was included at the exit pupil of the MOS which could be scanned across one quadrant of the MIRI pupil to measure the relative concentrations of the pupils associated with each of the MIRI optical subsystems.

The absolute flux calibration of the MTS was determined by modeling its optical throughput. This throughput estimate was embodied in a computer simulation, MTSSim, a program written in IDL to calculate the irradiance provided by the MTS at the MIRI input plane. MTSSim implemented a radiometric model of the MTS, with the hot source treated as a gray body with an emissivity of 95%. No diffraction effects were considered, and the system losses were limited to those caused by nonunity transmittance of the optical elements, as determined from subsystem measurements. Crucial to the accuracy of the end-to-end transmission budget was the error in estimating the transmission of the integrating sphere, since this could only be determined by geometrical modeling. As discussed in Glassey et al. (2015,

hereafter Paper IX), this uncertainty in the estimated efficiency of the MTS was regarded as consistent with the 55% difference seen when using it as a flux standard for measuring the throughput of MIRI, as compared with measurements of MIRI's subsystems.

9.2. Data Analysis

To provide a convenient reduction environment that was strictly configuration controlled and available to all of the international team, we developed the Data Handling and Analysis System (DHAS) (Morrison 2011).

The DHAS was based on a C++ analysis section, with a flexible IDL user interface. It first converts the raw integration ramps to slopes, subtracting the dark signals and correcting for nonlinearity. It also incorporates the best known algorithms to correct nonideal detector behavior, such as the reset anomaly (commonly seen in infrared arrays; the first samples after a reset are offset from the rest) (see Paper VIII for more discussion of non-ideal array behavior). It provides functions to display the resulting images and manipulate them, and also to organize the output of the MRS into a data cube.

The DHAS essentially implements the prototype for a MIRI data reduction pipeline. In addition to the continued use for instrument test data (e.g., at ISIM level), it is also being used to test and validate algorithms for the more sophisticated data reduction pipeline under development at STScI. The DHAS is also the means by which ongoing experiments on latent images, subarrays, annealing optimization, and other aspects of MIRI operations are evaluated.

10. SUMMARY

We have given a system level description of how MIRI provides its four key measurement functions to support a broad variety of *JWST* science objectives over the 5 to 28.5 μm spectral range. Details of these functions are described in Bouchet et al. (2015), Kendrew et al. (2015), Boccaletti et al. (2015), and Wells et al. (2015), but all share a common architecture described in this paper. Optomechanical subsystems are mounted to an isothermal structure which is thermally isolated from the *JWST* observatory and maintained at its operating temperature by a dedicated cooling system. These subsystems interface with the focal planes that are described in Ressler et al. (2015) and Rieke et al. 2015b. The MIRI Cooler, electrical system design, mechanisms, and control software have been presented. We have shown how the delivered instrument has balanced the conflicting needs of thermal isolation against those of stiffness under the mechanical loads experienced during launch, low electrical power dissipation, and limited mass and volume.

The control of molecular contamination is seen to be an important consideration for an instrument which will be at a significantly lower temperature than the rest of the observatory. The combination of a closeable cover and decontamination

heaters are designed to allow scientific performance to be maintained throughout the *JWST* mission. The provision of on-board calibration sources complements this approach to contamination control by allowing all major radiometric functions of the instrument to be measured accurately and repeatably without recourse to any external support equipment.

Flight Model testing of the integrated Optical System before and after delivery to NASA has demonstrated it to meet its key mechanical, thermal, and optical requirements. The success of the adopted approach for achieving the required alignment at cryogenic temperatures by designing and testing at ambient and cryogenic temperatures is notable. The timely and successful delivery to NASA was enabled by the inherent flexibility in the program that was provided by our coupling a modular approach to the build and test of subsystems with the choice of a three model (STM, VM, FM) system level solution for the integrated construction, qualification, and verification of the instrument performance.

The work presented is the effort of the entire MIRI team and the enthusiasm within the MIRI partnership is a significant factor in its success. MIRI draws on the scientific and technical expertise of the following organizations: Ames Research Center, USA; Airbus Defence and Space, UK; CEA-Irfu, Saclay, France; Centre Spatial de Liège, Belgium; Consejo Superior de Investigaciones Científicas, Spain; Carl Zeiss Optronics, Germany; Chalmers University of Technology, Sweden; Danish Space Research Institute, Denmark; Dublin Institute for Advanced Studies, Ireland; European Space Agency, Netherlands; ETCA, Belgium; ETH Zurich, Switzerland; Goddard Space Flight Center, USA; Institute d'Astrophysique Spatiale, France; Instituto Nacional de Técnica Aeroespacial, Spain; Institute for Astronomy, Edinburgh, UK; Jet Propulsion Laboratory, USA; Laboratoire d'Astrophysique de Marseille (LAM), France; Leiden University, The Netherlands; Lockheed Advanced Technology Center (USA); NOVA Opt-IR group at Dwingeloo, The Netherlands; Northrop Grumman, USA; Max Planck Institut für Astronomie (MPIA), Heidelberg, Germany; Laboratoire d'Etudes Spatiales et d'Instrumentation en Astrophysique (LESIA), France; Paul Scherrer Institut, Switzerland; Raytheon Vision Systems, USA; RUAG Aerospace, Switzerland; Rutherford Appleton Laboratory (RAL Space), UK; Space Telescope Science Institute, USA; Toegepast-Natuurwetenschappelijk Onderzoek (TNO-TPD), The Netherlands; UK Astronomy Technology Centre, UK; University College London, UK; University of Amsterdam, The Netherlands; University of Arizona, USA; University of Bern, Switzerland; University of Cardiff, UK; University of Cologne, Germany; University of Ghent; University of Groningen, The Netherlands; University of Leicester, UK; University of Leuven, Belgium; University of Stockholm, Sweden; Utah State University, USA. A portion of this work was carried out at the Jet Propulsion Laboratory, California Institute of Technology, under a contract with the National Aeronautics and Space Administration.

We would like to thank the following national and international funding agencies for their support of the MIRI development: NASA; ESA; Belgian Science Policy Office; Centre Nationale D'Etudes Spatiales (CNES); Danish National Space Centre; Deutsches Zentrum für Luft- und Raumfahrt (DLR); Enterprise Ireland; Ministerio De Economía y Competitividad; Netherlands Research School for Astronomy (NOVA); Netherlands Organisation for Scientific Research (NWO); Science and Technology Facilities Council; Swiss

Space Office; Swedish National Space Board; and UK Space Agency.

We take this opportunity to thank the ESA *JWST* Project team and the NASA Goddard ISIM team for their capable technical support in the development of MIRI, its delivery, and successful integration.

We are grateful for the comments of the external referee which helped us to improve the clarity of high-level description of the instrument in this paper.

REFERENCES

- Banks, K., Larson, M., Aymergen, C., & Zhang, B. 2008, Proc. SPIE, 7017, 8
- Belenguer, T., Alcacera, M. A., Aricha, A., Balado, A., Barandiarán, J., Bernardo, A., Canchal, M. R., Colombo, M., et al. 2008, Proc. SPIE, 7010, 39
- Bouchet, P., et al. 2015, PASP, 127, 612, Paper III
- Boccaletti, A., et al. 2015, PASP, 127, 633, Paper V
- Detre, Ö., Grözinger, U., Krause, O., et al. 2012, Proc. SPIE, 8450, 1 Z
- Glasse, A. et al. 2015, PASP, 127, 686, Paper IX
- Glasse, A., Lee, D., Parr-Burman, P., Hayton, D., & Mazy, E. 2006, Proc. SPIE, 6265, 100
- Glauser, A. M., et al. 2008, Proc. SPIE, 7018, 4 L
- Glauser, A. M., Langer, U., & Zehnder, A. 2009, Meas. Sci. Technol., 20, 5701
- Jessen, N. C., et al. 2004, Proc. SPIE, 5495, 23
- Kendrew, S., et al. 2015, PASP, 127, 623, Paper IV
- Krause, O., Müller, F., Birkmann, S., et al. 2010, Proc. SPIE, 7739, 37
- Morrison, J. 2011, in ASP Conf. Ser. 442, Astronomical Data Analysis and Software and Systems XX, ed. I. Evans (San Francisco: ASP), 399
- Radebaugh, Ray 2000, Proc. SPIE, 4130, 363
- Rieke, et al. 2015a, PASP, 127, 584, Paper I
- _____. 2015b, PASP, 127, 665, Paper VII
- Ressler, et al. 2015, PASP, 127, 675, Paper VIII
- Ross, R. G., Jr. 2004, in Cryocoolers 13, ed. R. G. Ross (New York: Springer), 15
- Scharton, T. D. 1997, NASA RP-1403
- Shaughnessy, B. M., Eccleston, P., Fereday, K. J., Canfer, S. J., Nørgaard-Nielsen, H. U., & Jessen, N. C. 2007, Cryogenics, 47, 348–352
- Shaughnessy, B. M., & Eccleston, P. 2009, 39th International Conference on Environmental Systems (ICES), Savannah, SAE Technical Paper 2009-01-2410
- Spradley, I. E., Nast, T. C., & Frank, D. J. 1990, Adv. Cryo. Eng., 35, 477
- Sykes, J., Eccleston, P., & Laine, B. 2012, in Proc. 12th European Conference on Spacecraft Structures, Materials, & Environmental Testing, SP-691, ed. L. Ouwehand (ESA), 159
- Wells, M., et al. 2015, PASP, 127, 646, Paper VI